Acquiring information about neutrino parameters by detecting supernova neutrinos

Ming-Yang Huang,[1,*] Xin-Heng Guo,[1,†] and Bing-Lin Young[2,3,‡]

[1]*College of Nuclear Science and Technology, Beijing Normal University, Beijing 100875, China*
[2]*Department of Physics and Astronomy, Iowa State University, Ames, Iowa 5001, USA*
[3]*Institute of Theoretical Physics, Chinese Academy of Sciences, Beijing 100190, China*

(Received 5 March 2010; published 19 August 2010)

We consider the supernova shock effects, the Mikheyev-Smirnov-Wolfenstein effects, the collective effects, and the Earth matter effects in the detection of type II supernova neutrinos on the Earth. It is found that the event number of supernova neutrinos depends on the neutrino mass hierarchy, the neutrino mixing angle θ_{13}, and neutrino masses. Therefore, we propose possible methods to identify the mass hierarchy and acquire information about θ_{13} and neutrino masses by detecting supernova neutrinos. We apply these methods to some current neutrino experiments.

DOI: 10.1103/PhysRevD.82.033011 PACS numbers: 14.60.Pq, 13.15.+g, 25.30.Pt, 26.30.−k

I. INTRODUCTION

Supernovas (SNs) are extremely powerful explosions in the Universe which terminate the life of some stars [1]. They make the catastrophic end of stars more massive than eight solar masses, leaving behind compact remnants such as neutron stars or black holes. The SN explosion, such as SN1987A [2], is one of the most spectacular comic events and the source of new physics ideas [3]. Detecting SN neutrinos on the Earth has been a subject of active investigation in astroparticle physics [1,2,4–8]. We may obtain some information about the explosion mechanism of SNs [5] and the parameters of neutrinos [4,6–8] by detecting SN neutrinos on the Earth. Several neutrino experiments, including the Daya Bay reactor neutrino underground laboratory [9], can be used to detect neutrino events from a SN explosion and serve as a SN early warning system [10].

Recently, several methods to obtain information on neutrino parameters by the study of SN neutrinos have been proposed. In Ref. [6], Dasgupta *et al.* proposed a method to identify the neutrino mass hierarchy for very small θ_{13} ($\sin^2\theta_{13} \leq 10^{-5}$) through the Earth matter effects. In Ref. [7], Skadhauge *et al.* proposed methods to identify the neutrino mass hierarchy for larger θ_{13} ($\sin^2\theta_{13} \geq 10^{-4}$) and obtain information about θ_{13} by SN neutrinos. In Ref. [8], using the event number of the delayed SN neutrinos, a method to measure neutrino masses was proposed by Beacom *et al.*. In these works, the SN shock effects and the collective effects were not taken into account. Furthermore, uncertainties of some of the parameters appearing in SN neutrino fluxes, such as the luminosities L^0_α, temperatures T_α, and pinching parameters η_α, were not considered.

In Ref. [11], we studied the Earth matter effects in the detection of SN neutrinos at the Daya Bay experiment and proposed a possible method to acquire information about the neutrino mixing angle θ_{13} smaller than 1.5° which is difficult to access in reactor neutrino experiments. We defined the ratio R as the event number of ν_e over that of $\bar{\nu}_e$. Using the relation between the event number of SN neutrinos N and θ_{13}, we can obtain information about small θ_{13} by measuring R. In that paper, a simplified picture for the collective effects was used [12] and the neutrino flavor transformation due to the SN shock effects was not considered. Furthermore, it was assumed that different flavor SN neutrinos have the same time-independent luminosity. Hence in that calculation there are several uncertainties which we will address in the present work.

In this paper, we study the collective effects more accurately [13,14] and consider the neutrino flavor transformation arising from the SN shock effects [15–17]. In addition, according to current Monte Carlo simulations on SN neutrino spectra [18], we allow different flavor neutrinos to have different time-dependent luminosities. Furthermore, in order to reduce the uncertainties of unknown parameters in SN neutrino fluxes such as luminosity, temperature, and pinching parameter, we will define the ratio of the event number of SN neutrinos for the charged-current reaction detected after 1 s over that detected before 1 s (this is different from the ratio considered in Ref. [11]). With this ratio, we may identify the mass hierarchy, $\Delta m^2_{31} > 0$ vs $\Delta m^2_{31} < 0$, and acquire information about θ_{13}. This method can be applied to neutrino detectors of various types. Examples are the liquid scintillator detector of the Daya Bay experiment [9] under construction, the decommissioned heavy water detector of the previous Sudbury Neutrino Observatory (SNO) [19], etc.

The other main purpose of the present work is to propose a method to obtain some information about neutrino masses from SN neutrinos. Since neutrinos have small masses, their transmit velocities are smaller than that of light. Therefore, a massive neutrino will have an energy- and mass-dependent delay relative to a massless neutrino

*hmy19151905@mail.bnu.edu.cn
†Corresponding author
xhguo@bnu.edu.cn
‡young@iastate.edu

after traveling over a long distance [8]. We will define another ratio, for the neutral-current reactions, as the event number of the delayed SN neutrinos over the total event number. With the relation between this ratio and neutrino masses, we will propose a possible method to acquire information about neutrino masses. This method will also be applied to Daya Bay and SNO for examples.

The paper is organized as follows. In Sec. II, we review the detection of SN neutrinos on the Earth. In Sec. III, we propose a possible method to identify the mass hierarchy and acquire information about θ_{13} and apply the method to the Daya Bay and SNO experiments. In Sec. IV, a method to acquire information about neutrino masses is given and also applied to Daya Bay and SNO. A summary is given in Sec. V.

II. DETECTION OF SN NEUTRINOS ON THE EARTH

In the explosion a typical type II SN generates intensive neutrinos which carry about 99% of the total energy and the explosion itself consumes about 1% of the total energy. The vast amount of neutrinos is produced in two bursts. In the first burst which lasts for only a few milliseconds, electron neutrinos are generated by the electron capture by nuclei $e^- + N(Z, A) \rightarrow N(Z-1, A) + \nu_e$ via the inverse beta decay $e^- + p \rightarrow n + \nu_e$ which leads to a neutron rich star. In the second burst which lasts longer (about 10 seconds), neutrinos of all flavors are produced through the electron-positron pair annihilation $e^- + e^+ \rightarrow \nu_\alpha + \bar{\nu}_\alpha$, the electron-nucleon bremsstrahlung $e^\pm + N \rightarrow e^\pm + N + \nu_\alpha + \bar{\nu}_\alpha$, the nucleon-nucleon bremsstrahlung $N + N \rightarrow N + N + \nu_\alpha + \bar{\nu}_\alpha$, the plasmon decay $\gamma \rightarrow \nu_\alpha + \bar{\nu}_\alpha$, and the photoannihilation $\gamma + e^\pm \rightarrow e^\pm + \nu_\alpha + \bar{\nu}_\alpha$ [20].

We assume a ''standard'' SN explosion at a distance $D = 10$ kpc from the Earth, releasing a total energy $E_B = 3 \times 10^{53}$ erg (similar to SN1987A) and the luminosity flux of the SN neutrino α, L_α, distributed in time as [21–23]

$$L_\alpha(t) = L_\alpha^0 e^{-t/\tau}, \tag{1}$$

where L_α^0 is the luminosity of the neutrino α at $t = 0$ and τ the luminosity decay time. The following range of τ was obtained by fitting the experimental data of SN1987A with the exponentially decaying luminosity [21,22]:

$$\tau = 1.74\text{–}4.19 \text{ s}. \tag{2}$$

The typical relations among L_α^0 obtained from numerical simulations are [18]

$$\begin{aligned} &\frac{L_{\nu_e}^0}{L_{\nu_x}^0} = (0.5\text{–}2), \qquad L_{\nu_e}^0 = L_{\bar{\nu}_e}^0, \\ &L_{\nu_x}^0 = L_{\bar{\nu}_x}^0, \qquad (x = \mu, \tau). \end{aligned} \tag{3}$$

There are two parametrizations of SN neutrino fluxes used in general simulations, one used by the Livermore group [24,25] and the other by the Garching group [18]. In the present work, we use the Livermore parametrization which is similar to the Fermi-Dirac distribution. For the SN neutrino of flavor α, the time-integrated neutrino energy spectra is given by [25]

$$F_\alpha^{(0)}(E) = \frac{L_\alpha}{F_{\alpha 3} T_\alpha^4} \frac{E^2}{\exp(E/T_\alpha - \eta_\alpha) + 1}, \tag{4}$$

where E is the neutrino energy, T_α the temperature of the neutrino α, η_α the pinching parameter of the spectrum, L_α the luminosity given by Eq. (1), and $F_{\alpha j}$ is defined by

$$F_{\alpha j} = \int_0^\infty \frac{x^j}{\exp(x - \eta_\alpha) + 1} dx,$$

where j is an integer. The spectra obtained from numerical simulations can be well fitted by [26]

$$\begin{aligned} &T_{\nu_e} = 3\text{–}4 \text{ MeV}, \qquad T_{\bar{\nu}_e} = 5\text{–}6 \text{ MeV}, \\ &T_{\nu_x} = T_{\bar{\nu}_x} = 7\text{–}9 \text{ MeV}, \qquad \eta_{\nu_e} \approx 3\text{–}5, \\ &\eta_{\bar{\nu}_e} \approx 2.0\text{–}2.5, \qquad \eta_{\nu_x} = \eta_{\bar{\nu}_x} \approx 0\text{–}2. \end{aligned} \tag{5}$$

While neutrinos propagate outward to the surface of the SN they could be subjected to the SN shock effects [16,17,27–29], the Mikheyev-Smirnov-Wolfenstein (MSW) effects [30–32], and the collective effects [12,14,33–39]. Then, after traveling the cosmic distance to reach the Earth, they go through a part of the Earth and are subjected to the Earth matter effects [40–43]. In the following, we will consider the above four types of effects in detail.

A. Time dependence of the signal: SN shock effects

As was pointed out in Ref. [16], the shock propagating inside the SN may reach the region of densities relevant for neutrino conversion during the period of neutrino emission. It modifies the density profile of the star, thus affecting neutrino flavor transitions after the core bounce [16,17]. The time-dependent variations of the neutrino potential in matter along with the SN shock profile can leave distinctive imprints on the energy and time structure of the neutrino signal. The study of such effects may provide us with additional constraints for the determination of the neutrino mass hierarchy, the neutrino mixing angle θ_{13}, and neutrino masses.

In Ref. [17], the authors introduce a simplified, empirical parametrization of the shock density profile ρ, which reproduces the main features of the graphical profile of Ref. [16] and is continuous in both t and the supernova radial coordinate r. In this way, numerical and analytical calculations of the crossing probability at the high resonance region P_H can continuously cover the relevant parameter space. We follow the notation of Ref. [17] in the discussion below.

For postbounce time $t < 1$ s [44] before the shock effects begin, the SN matter density is

$$\rho_0(r) \backsimeq 10^{14} \cdot \left(\frac{r}{1\ \mathrm{km}}\right)^{-2.4}\ \mathrm{g/cm^3}. \tag{6}$$

For $t \geq 1$ s the shock effects set in and the matter density is given by

$$\rho(r,t) = \rho_0(r) \cdot \begin{cases} \xi \cdot f(r,t) & (r \leq r_s) \\ 1 & (r > r_s) \end{cases}, \tag{7}$$

where $f(r,t)$ is defined as

$$f(r,t) = \exp\{[0.28 - 0.69\ln(r_s/\mathrm{km})] \times [\arcsin(1 - r/r_s)]^{1.1}\}, \tag{8}$$

and ξ is a typical ratio of the potential across the shock front,

$$\xi = V_+/V_- \backsimeq 10, \tag{9}$$

which measures the SN matter potential $V(r)$ drop from

$$V_+ = \lim_{r \to r_s^-} V(r) \tag{10}$$

to

$$V_- = \lim_{r \to r_s^+} V(r). \tag{11}$$

The SN matter potential is related to the SN electron density $N_e(r)$ by

$$V(r) = \sqrt{2} G_F N_e(r) = \sqrt{2} G_F N_A \rho(r) Y_e, \tag{12}$$

where N_A is Avogadro's number and Y_e is the electron fraction. In the numerical calculations, we assume $Y_e = 0.5$. In Eqs. (6)–(9), a slightly accelerating shock-front position r_s is assumed with the explicit time dependence

$$r_s(t) = -4.6 \times 10^3 + 1.13 \times 10^4 \cdot t + 1 \times 10^2 \cdot t^2, \tag{13}$$

where r_s is in units of km and t in units of s.

Using Eqs. (6)–(9), we plot in Fig. 1 the density profile of the SN as a function of the radius at different times. These curves reproduce reasonably well the main features of the shock profiles as shown in Ref. [16]. The straight line labeled by $t = 0$ is the unmodified density profile given by Eq. (6). Once the shock effects begin, at a given time the shock radius r_s is determined by Eq. (13). The density profile is suppressed more and more in the region $r < r_s$ as the time and therefore r_s increase. The density reaches a minimum and then rises relatively quickly to the value $\xi\rho_0(r_s)$ as $r \to r_s^-$. In the region $r > r_s$ the density profile is the unperturbed original form ρ_0. The density suffers a sizable discontinuity at r_s.[1] Neutrinos emitted in the region $r > r_s$, because their velocities (near the speed of the light) are much higher than that of the shock wave propagation (which is the order of 10^4 km/s), are not influenced by the shock effects. Hence the majority of SN neutrinos which are emitted within a 10 s period will be able to assemble the whole range of the profile of the SN density under the influence of the shock. An important consequence of the density modification by the shock wave is that some of the neutrinos can undergo multiple resonance flavor conversion when they traverse the SN. We consider them below.

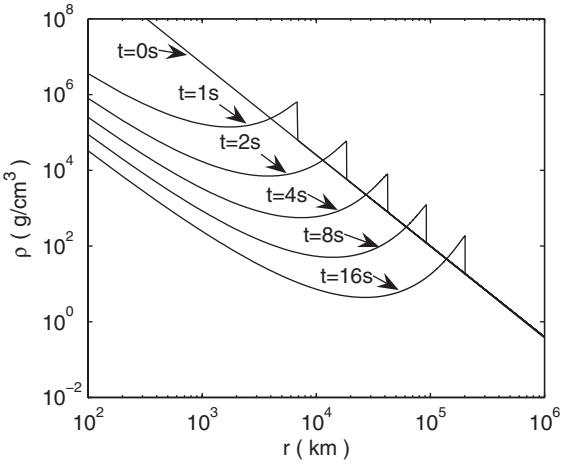

FIG. 1. The density of the SN as a function of the radius r at different times.

Let us first consider the neutrino flavor conversion due to the density discontinuity at the shock front r_s. This crossing probability of the neutrino flavor transformation which we denote as P_s can be determined by the conservation of flavor across the matter potential discontinuity. By a simple calculation, we have [31]

$$P_s = \sin^2(\theta_m^+ - \theta_m^-), \tag{14}$$

where θ_m^+ and θ_m^- are, respectively, the effective mixing angles in matter immediately before and after the shock-front position r_s. Such angles are defined by

$$\cos 2\theta_m^\pm = \frac{\Delta m_{31}^2 \cos 2\theta_{13} - 2EV^\pm}{\sqrt{(\Delta m_{31}^2 \cos 2\theta_{13} - 2EV^\pm)^2 + (\Delta m_{31}^2 \sin 2\theta_{13})^2}}. \tag{15}$$

B. MSW effects

The MSW effects [30] are the adiabatic or partially adiabatic neutrino flavor conversion in media with locality or time varying matter density. The main feature is that in a high density medium a flavor is also a mass state which propagates without flavor oscillation, until crossing a resonance where there is a finite probability for flavor change, i.e., a jump from one mass eigenstate to another. For θ_{13} smaller than 3°, using the Landau-Zener formula [45], one can obtain the crossing probability P_{Hi} for neutrinos to

[1] It can be shown that $f(r_s, t) = 1$ and therefore the discontinuity is $(\xi - 1)\rho_0(r_s) \approx 9\rho(r_s)$.

jump from one mass eigenstate to another at the high resonance layer ($r = r_i$)

$$P_{Hi} = \exp\left(-\frac{\pi}{2}\gamma\right), \tag{16}$$

with

$$\gamma = \frac{|\Delta m^2_{31}|}{2E}\frac{\sin^2 2\theta_{13}}{\cos 2\theta_{13}}\frac{1}{|d\ln N_e/dr|_{\rm res}}, \tag{17}$$

where N_e is the electron density [31] and $|\Delta m^2_{31}| \backsimeq |\Delta m^2_{32}| \backsimeq 2.4 \times 10^{-3}$ eV^2 [46]. Similarly, one can calculate the expression of the crossing probability P_L at the low resonance region inside the SN. However, due to the large angle solution of the solar neutrino, $P_L \simeq 0$.

In the presence of a propagating shock wave, the calculation of the global crossing probability P_H is not straightforward. The shock modifies the density profile as discussed in the preceding subsection. Within the shock wave and near the shock front, the matter density is no longer monotonically decreasing, but rather goes through a minimum and a maximum. So the resonance condition can satisfy possibly as many as three points:

$$\Delta m^2_{31} \cdot \cos 2\theta_{13} = 2\sqrt{2} G_F N_e(r_i) E, \qquad (i = 1, 2, 3). \tag{18}$$

It is, of course, possible that there are only two or one resonance points, or even none at all. In the case of three resonance points, which we denote as r_i, $i = 1, 2, 3$, two of the points lie below the shock front and the third one beyond the shock front, i.e., $r_1 < r_2 < r_s < r_3$. The crossing probability P_{Hi} at r_i, $i = 1, 2, 3$, can be calculated from Eq. (16). Note that although the matter densities are the same at all resonance points as required by Eq. (18), their crossing probabilities, as given by Eq. (17), may be different because the slope of the matter density may be different at different resonance points. The global crossing probability can be expressed in terms of four crossing probabilities P_{H1}, P_{H2}, P_s, and P_{H3}.

To obtain the expressions of the global crossing probabilities, we first define four densities: $\rho_{\rm res}$ is the resonance density which satisfies Eq. (18), ρ_+ the density at $r = r_s$ corresponding to the matter potential V_+, ρ_- the density at $r = r_s$ corresponding to the matter potential V_-, and ρ_b the density at the bottom of the camber which is the minimum of the density profile below the shock front. From Fig. 1, it can be seen that

$$\rho_+ > \rho_-, \qquad \rho_+ > \rho_b.$$

In the prebounce time period $t < 1$ s, the resonance condition occurs at only one point and there are no neutrino shock effects. Then,

$$P_H = P_{H3}. \tag{19}$$

In the postshock period $t \geq 1$ s we have four different situations:

(1) For $\rho_- < \rho_{\rm res} < \rho_b$, the resonance condition does not occur and then

$$P_H = P_s. \tag{20}$$

(2) For $\rho_{\rm res} > \rho_+$, or $\rho_{\rm res} = \rho_b$ and $\rho_{\rm res} > \rho_-$, or $\rho_{\rm res} < \rho_b$ and $\rho_{\rm res} \leq \rho_-$, the resonance condition occurs at only one point, $r = r_1$ or $r = r_3$, and then

$$P_H = P_{Hk} + P_s - 2P_{Hk}P_s + 2\sqrt{P_{Hk}P_s(1 - P_{Hk})(1 - P_s)}\cos\phi_{ks}, \quad (k = 1, 3). \tag{21}$$

(3) For $\rho_b < \rho_{\rm res} \leq \rho_+$ and $\rho_{\rm res} > \rho_-$, or $\rho_{\rm res} = \rho_b$ and $\rho_{\rm res} \leq \rho_-$, the resonance condition occurs at two points, $r = r_1$, r_2 or $r = r_1$, r_3, and then

$$\begin{aligned} P_H = {} & (P_{H1} + P_{Hl} + P_s) - 2(P_{H1}P_{Hl} + P_{H1}P_s + P_{Hl}P_s) + 4P_{H1}P_{Hl}P_s \\ & + 2(1 - 2P_s)\sqrt{P_{H1}P_{Hl}(1 - P_{H1})(1 - P_{Hl})}\cos\phi_{1l} + 2(1 - 2P_{H1})\sqrt{P_{Hl}P_s(1 - P_{Hl})(1 - P_s)}\cos\phi_{ls} \\ & + 2(1 - 2P_{Hl})\sqrt{P_{H1}P_s(1 - P_{H1})(1 - P_s)}\cos\phi_{1s} \qquad (l = 2, 3). \end{aligned} \tag{22}$$

(4) For $\rho_b < \rho_{\rm res} \leq \rho_-$, the resonance condition occurs at three points, $r = r_1$, r_2, r_3, and then

TABLE I. Summary of neutrino flavor conversions due to the neutrino shock effects and the MSW effects in various density regions.

$t < 1$ s	$t \geq 1$ s			
P_{H3}	$\rho_b > \rho_-$		$\rho_- \geq \rho_b$	
	Resonance in region	Flavor conversion involved	Resonance in region	Flavor conversion involved
	$\rho_{\rm res} > \rho_+$	P_{H1}, P_s	$\rho_{\rm res} > \rho_+$	P_{H1}, P_s
	$\rho_+ \geq \rho_{\rm res} > \rho_b$	P_{H1}, P_{H2}, P_s	$\rho_+ \geq \rho_{\rm res} > \rho_-$	P_{H1}, P_{H2}, P_s
	$\rho_{\rm res} = \rho_b$	P_{H1}, P_s	$\rho_- \geq \rho_{\rm res} > \rho_b$	P_{H1}, P_{H2}, P_s, P_{H3}
	$\rho_b > \rho_{\rm res} > \rho_-$	P_s	$\rho_{\rm res} = \rho_b$	P_{H1}, $P_s P_{H3}$
	$\rho_- \geq \rho_{\rm res}$	P_s, P_{H3}	$\rho_b > \rho_{\rm res}$	P_s, P_{H3}

$$
\begin{aligned}
P_H = {} & (P_{H1} + P_{H2} + P_s + P_{H3}) - 2(P_{H1}P_{H2} + P_{H1}P_{H3} + P_{H1}P_s + P_{H2}P_{H3} + P_{H2}P_s + P_{H3}P_s) \\
& + 4(P_{H1}P_{H2}P_{H3} + P_{H1}P_{H2}P_s + P_{H1}P_{H3}P_s + P_{H2}P_{H3}P_s) - 8P_{H1}P_{H2}P_{H3}P_s \\
& + 2(1 - 2P_s - 2P_{H3} + 4P_{H3}P_s)\sqrt{P_{H1}P_{H2}(1 - P_{H1})(1 - P_{H2})}\cos\phi_{12} \\
& + 2(1 - 2P_{H1} - 2P_{H3} + 4P_{H1}P_{H3})\sqrt{P_{H2}P_s(1 - P_{H2})(1 - P_s)}\cos\phi_{2s} \\
& + 2(1 - 2P_{H2} - 2P_{H3} + 4P_{H2}P_{H3})\sqrt{P_{H1}P_s(1 - P_{H1})(1 - P_s)}\cos\phi_{1s} \\
& + 2(1 - 2P_{H1} - 2P_{H2} + 4P_{H1}P_{H2})\sqrt{P_{H3}P_s(1 - P_{H3})(1 - P_s)}\cos\phi_{s3} \\
& + 2(1 - 2P_s - 2P_{H1} + 4P_{H1}P_s)\sqrt{P_{H2}P_{H3}(1 - P_{H2})(1 - P_{H3})}\cos\phi_{23} \\
& + 2(1 - 2P_s - 2P_{H2} + 4P_{H2}P_s)\sqrt{P_{H1}P_{H3}(1 - P_{H1})(1 - P_{H3})}\cos\phi_{13} \\
& - 8\sqrt{P_{H1}P_{H2}(1 - P_{H1})(1 - P_{H2})}\cos\phi_{12}\sqrt{P_{H3}P_s(1 - P_{H3})(1 - P_s)}\cos\phi_{s3}. \qquad (23)
\end{aligned}
$$

In Eqs. (21)–(23), ϕ_{ij} is defined as

$$\phi_{ij} \approx \int_{r_i}^{r_j} dx \frac{1}{2E}\sqrt{[\Delta m_{31}^2 \cos 2\theta_{13} - 2EV(r)]^2 + (\Delta m_{31}^2 \sin 2\theta_{13})^2}, \qquad (24)$$

with $V(r)$ being the SN matter potential. A summary for neutrino flavor conversions due to the neutrino shock effects and the MSW effects in various density regions is given in Table I. Because of the SN matter effects and the SN shock effects, the expressions of P_H, Eqs. (19)–(23), are different from Eq. (25) in Ref. [17] and Eq. (34) in Ref. [33].

Because of the various effects they have been subjected to, the SN neutrinos reaching the Earth have very rich structures to be explored in their spectra in time, energy, and the mixing angle θ_{13}. In Fig. 2, we plot the crossing probability P_H as a function of the neutrino energy E at $t = 4$ s for two very small mixing angles $\sin^2\theta_{13} = 10^{-5}$ and 10^{-4}. It is seen that there are large variations in P_H as the neutrino energy varies. These forms of behavior are different from those given in Refs. [11,17]. In Fig. 3, we plot P_H as a function of t for $\sin^2\theta_{13} = 10^{-4}$ at a fixed E for three different values of E. It can be seen that the shapes of the curves depend strongly on E and there are many oscillations in P_H in an interval around $t = 5$ s. The interval enlarges and moves to higher t value as E increases. This is different from that given in Ref. [17]. In Fig. 4, we plot P_H as a function of θ_{13} for different values of E and t. It is found that at some values of θ_{13}, which depends on the energy of SN neutrinos, P_H begins to change very rapidly with θ_{13} at $t = 4$ s, and the behavior of the P_H dependence on θ_{13} is different from that given in Ref. [11]. These differences are attributable to the different SN matter effects when the shock effects are included in the consid-

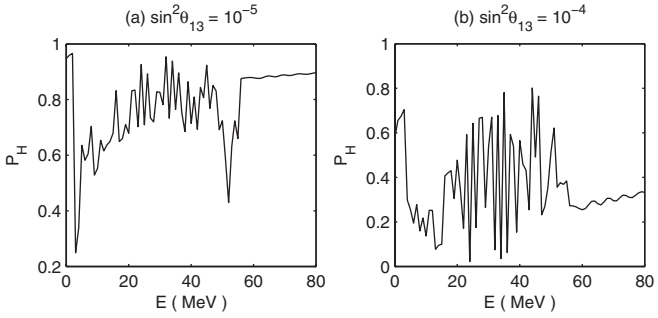

FIG. 2. The crossing probability at the high resonance region P_H as a function of the neutrino energy E for two very small neutrino mixing angles θ_{13} at $t = 4$ s.

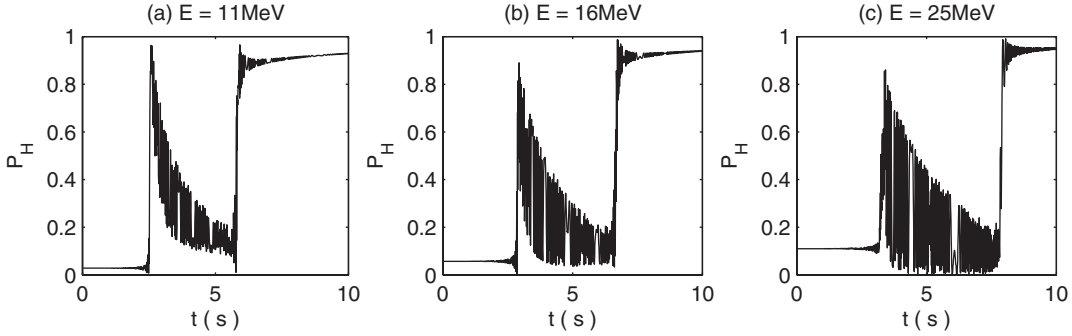

FIG. 3. The crossing probability at the high resonance region P_H as a function of time t for three different neutrino energies at $\sin^2\theta_{13} = 10^{-4}$.

eration. The relation between P_H and θ_{13} will provide a way to obtain information on θ_{13} and the study of the shock wave effects.

C. Neutrino-neutrino interactions: Collective effects

Because of the neutrino-neutrino forward scattering or neutrino self-interaction, neutrinos can experience collective flavor transformation in the SN near the neutrinosphere where the neutrino number densities are very large [35]. This phenomenon is different from the MSW effects in that the flavor evolution histories of neutrinos in the collective oscillations are coupled together and must be solved simultaneously.

Recently, a significant amount of study on collective effects has been made by a number of authors, e.g., Duan *et al.* [33–36], Dasgupta *et al.* [6,12], Hannestad *et al.* [37], Raffelt *et al.* [38], and Fogli *et al.* [39]. Defining $P_{\nu\nu}(\bar{P}_{\nu\nu})$ as the probability that the (anti)neutrino $\nu(\bar{\nu})$ remains as $\nu(\bar{\nu})$ after the collective effects, Dasgupta *et al.* [6] introduced a much simplified picture to explain the characteristics of the collective effects which we followed in our earlier paper [11], i.e., $P_{\nu\nu} = \bar{P}_{\nu\nu} = 1$ in the case of normal mass hierarchy; and $\bar{P}_{\nu\nu} = 1$,

$$P_{\nu\nu} = \begin{cases} 1 & (E < E_C) \\ 0 & (E > E_C) \end{cases},$$

in the case of inverted mass hierarchy, where E_C is a critical energy across which a stepwise flavor conversion of ν_e develops. However, from the numerical simulations of the collective effects obtained by Duan *et al.* [14], it is found that $P_{\nu\nu}(\bar{P}_{\nu\nu})$ depends on the neutrino (antineutrino) energy E, the SN radial coordinate r, the SN neutrino emission angle, and it is very difficult to obtain an analytical expression for $P_{\nu\nu}(\bar{P}_{\nu\nu})$. It can be seen from movies 5 and 6[2] at [47] and in Ref. [14] that when the SN radial coordinate r increases, there are oscillations between ν_e ($\bar{\nu}_e$) and ν_τ ($\bar{\nu}_\tau$) due to the collective effects. When $r \geq$ 220 km, which is far away from the neutrinosphere, the collective effects for the neutrino amount to a swap between the ν_e and ν_τ fluxes, irrespective of the mass hierarchy being normal or inverted. For the antineutrino, in the case of normal mass hierarchy, the fluxes of $\bar{\nu}_e$ and $\bar{\nu}_\tau$ are nearly unchanged and there is no swap between them. In the case of inverted mass hierarchy, the behaviors of the $\bar{\nu}_e$ and $\bar{\nu}_\tau$ fluxes are very complex and, for simplicity, they are generally approximated [13,35] because there is no swap between them. In this way, we apply the following new simplified picture to describe the characteristics of the collective effects:

$$P_{\nu\nu} = \begin{cases} 1 & (E < E_C) \\ 0 & (E > E_C) \end{cases}, \tag{25}$$

for neutrinos and

$$\bar{P}_{\nu\nu} = 1, \tag{26}$$

for antineutrinos. It will be seen from our numerical calculations that the results obtained in Secs. III and IV hardly change for E_C varying between 6 MeV and 10 MeV. Therefore, similar to Ref. [13], we take $E_C = 10$ MeV.

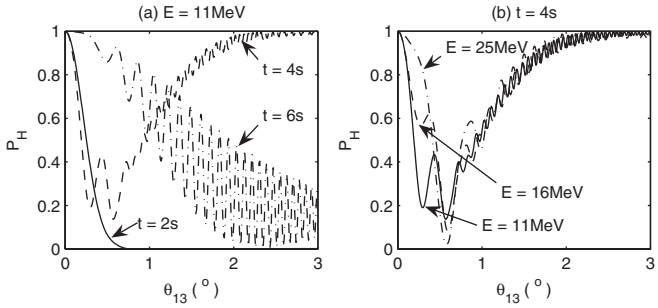

FIG. 4. The crossing probability at the high resonance region P_H as a function of the neutrino mixing angle θ_{13}: (a) for three different times at $E = 11$ MeV. The solid, dashed, and dotted curves are for $t = 2$ s, 4 s, 6 s, respectively; (b) for three different neutrino energies at $t = 4$ s. The solid, dashed, and dotted curves are for $E = 11$ MeV, 16 MeV, 25 MeV, respectively.

[2]Movies 5 and 6 which describe the full simulation of the collective effects [14] are available at [47].

D. Earth matter effects

Neutrinos from a SN may travel through a significant portion of the Earth before reaching the detector and are subjected to the matter effects [40]. Therefore, we need to consider the Earth matter effects in studying SN neutrinos. Suppose a neutrino reaches the detector at the incident angle θ (see Fig. 5). Then the distance that the neutrino travels through the Earth to the detector L and the distance of the neutrino to the center of the Earth $\tilde{x}$ are given by

$$L = (-R_E + h)\cos\theta + \sqrt{R_E^2 - (R_E - h)^2\sin^2\theta},$$
$$\tilde{x} = \sqrt{(-R_E + h)^2 + (L - x)^2 + 2(R_E - h)(L - x)\cos\theta},$$

where h is the depth of the detector in the Earth, x the distance that the neutrino travels into the Earth, and R_E the radius of the Earth.

Let P_{ie} be the probability that a neutrino mass eigenstate ν_i enters the surface of the Earth and arrives at the detector as an electron neutrino ν_e; then we have [42]

$$P_{2e} = \sin^2\theta_{12} + \frac{1}{2}\sin^2 2\theta_{12}\int_{x_0}^{x_f} dx V(x)\sin\phi^m_{x\to x_f}, \quad (27)$$

where $V(x)$ is the potential ν_e experiences due to the matter density $\rho(x)$ inside the Earth [11,42,48]

$$V(x) = \sqrt{2}G_F N_A \rho(x) Y_e, \quad (28)$$

and $\phi^m_{a\to b}$ is defined as

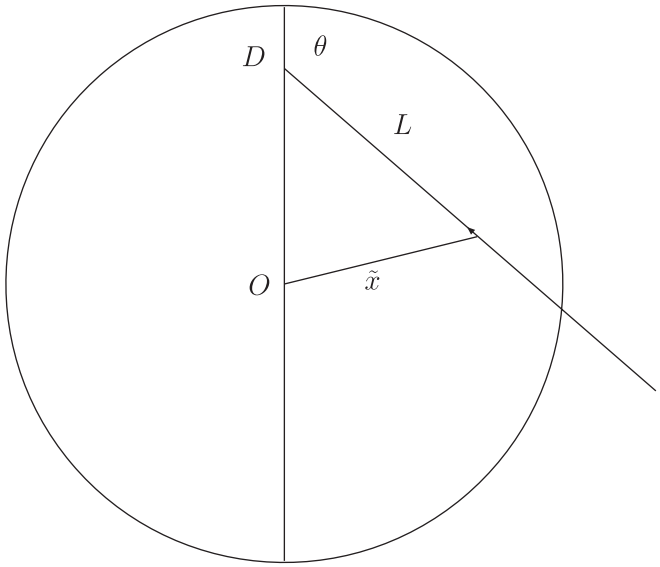

FIG. 5. Illustration of the path of the SN neutrino reaching the detector in the Earth. D is the location of the detector, θ is the incident angle of the neutrino, O is the center of the Earth, L is the distance the neutrino travels through the Earth matter, and $\tilde{x}$ is the instantaneous distance of the neutrino to the center of the Earth.

$$\phi^m_{a\to b} = \int_a^b dx\Delta_m(x),$$

where

$$\Delta_m(x) = \frac{\Delta m^2_{21}}{2E}\sqrt{(\cos 2\theta_{12} - \varepsilon(x))^2 + \sin^2 2\theta_{12}}, \quad (29)$$

with $\theta_{12} \backsimeq 34.5°$, $\Delta m^2_{21} = 7.7\times 10^{-5}$ eV^2, $\varepsilon(x) = 2EV(x)/\Delta m^2_{21}$ [46].

E. Summary of all matter effects

When all the effects, including the shock, MSW, collective, and the Earth matter, are taken into account, the SN neutrino fluxes at the detector can be written as

$$\begin{aligned} F^D_{\nu_e} &= pF^{(0)}_{\nu_e} + (1-p)F^{(0)}_{\nu_x}, \\ F^D_{\bar{\nu}_e} &= \bar{p}F^{(0)}_{\bar{\nu}_e} + (1-\bar{p})F^{(0)}_{\bar{\nu}_x}, \\ 2F^D_{\nu_x} &= (1-p)F^{(0)}_{\nu_e} + (1+p)F^{(0)}_{\nu_x}, \\ 2F^D_{\bar{\nu}_x} &= (1-\bar{p})F^{(0)}_{\bar{\nu}_e} + (1+\bar{p})F^{(0)}_{\bar{\nu}_x}, \end{aligned} \quad (30)$$

where the survival probabilities p and $\bar{p}$ are given by

$$\begin{aligned} p &= P_{2e}[P_H P_{\nu\nu} + (1-P_H)(1-P_{\nu\nu})], \\ \bar{p} &= (1-\bar{P}_{2e})\bar{P}_{\nu\nu}, \end{aligned} \quad (31)$$

for the normal mass hierarchy and

$$\begin{aligned} p &= P_{2e}P_{\nu\nu}, \\ \bar{p} &= (1-\bar{P}_{2e})[\bar{P}_H\bar{P}_{\nu\nu} + (1-\bar{P}_H)(1-\bar{P}_{\nu\nu})], \end{aligned} \quad (32)$$

for the inverted mass hierarchy.

Therefore, the event numbers $N(i)$ of SN neutrinos in the various reaction channels "i" can be calculated by integrating over the neutrino energy, the product of the target number N_T, the cross section of the given channel $\sigma(i)$, and the neutrino flux function at the detector F^D_α,

$$N(i) = N_T\int dE\cdot\sigma(i)\cdot\frac{1}{4\pi D^2}\cdot F^D_\alpha, \quad (33)$$

where α stands for the neutrino or antineutrino of a given flavor, and D is the distance between the SN and the Earth. In the following section, we propose a method to identify the mass hierarchy and acquire information about θ_{13} by detecting SN neutrinos.

III. IDENTIFY THE MASS HIERARCHY AND ACQUIRE INFORMATION ABOUT θ_{13} BY DETECTING SN NEUTRINOS

In the above section, we discussed the SN shock effects, the MSW effects, the collective effects, and the Earth matter effects in detail for the detection of SN neutrinos. From Eqs. (14)–(17) and (19)–(33), it can be seen that the event number of SN neutrinos depends on the mixing angle θ_{13} for different mass hierarchies. Therefore, we may

identify the mass hierarchy and acquire information about θ_{13} by detecting SN neutrinos. In Ref. [11], we defined a ratio of the event number of ν_e over that of $\bar{\nu}_e$ and studied the method to acquire information about θ_{13}. However, in that paper, we ignored the SN shock effects and only a very simple model for the collective effects was considered. In addition, with the naive luminosity of SN neutrinos employed there, the uncertainties in θ_{13} will be very large. In the present work, we take into account the SN shock effects and consider the collective effects more realistically. In order to further reduce the influence of the uncertainties in the parameters of the SN neutrino fluxes, we define a more appropriate ratio as the event number of SN neutrinos for the charged-current reaction detected after 1 s over that detected before 1 s. Using this new ratio, we can better acquire information about θ_{13} and identify the neutrino mass hierarchy. From Ref. [11] and detailed numerical studies related to the present work, we found that the ratios of event numbers of SN neutrinos are nearly independent of the SN neutrino incident angle. Therefore, in the following we will only consider the case for the incident angle of 30°.

There will be eight detectors located at the near and far sites of the Daya Bay experiment [9]. The total detector mass is about 300 tons and the depth of the detector $h \backsimeq 400$ m. The Daya Bay Collaboration has decided to use linear alkyl benzene (LAB) as the main part of the liquid scintillator. LAB has a chemical composition including C and H and the ratio of the number of C and H is about 0.6. Then, the total numbers of target protons, electrons, and ^{12}C are

$$N_T^{(p)} = 2.20 \times 10^{31}, \qquad N_T^{(e)} = 1.01 \times 10^{32},$$
$$N_T^{(C)} = 1.32 \times 10^{31}.$$

In the Daya Bay experiment, there are three reactions which can be used to detect SN neutrinos: the inverse beta decay, neutrino-electron reactions, and neutrino-carbon reactions. However, since the event number observed in the channel of neutrino-electron reactions at Daya Bay is very small [11], these reactions will not be considered in the present work. Therefore, we only consider the inverse beta decay and the neutrino-carbon reactions; their effective cross sections are given as follows [49,50]:

(1) The inverse beta decay is

$$\sigma(\bar{\nu}_e p) = 9.5 \times 10^{-44} (E\ (\mathrm{MeV}) - 1.29)^2\ \mathrm{cm}^2, \tag{34}$$

where the reaction threshold is $E_{\mathrm{th}} = 1.80$ MeV.

(2) The neutrino-carbon reactions are

$$\langle \sigma(^{12}\mathrm{C}(\nu_e, e^-)^{12}\mathrm{N}) \rangle = 1.85 \times 10^{-43}\ \mathrm{cm}^2,$$
$$\langle \sigma(^{12}\mathrm{C}(\bar{\nu}_e, e^+)^{12}\mathrm{B}) \rangle = 1.87 \times 10^{-42}\ \mathrm{cm}^2, \tag{35}$$

for the charged-current capture, and

$$\langle \sigma(\nu_e\, ^{12}\mathrm{C}) \rangle = 1.33 \times 10^{-43}\ \mathrm{cm}^2,$$
$$\langle \sigma(\bar{\nu}_e\, ^{12}\mathrm{C}) \rangle = 6.88 \times 10^{-43}\ \mathrm{cm}^2,$$
$$\langle \sigma(\nu_{\mu,\tau}(\bar{\nu}_{\mu,\tau})^{12}\mathrm{C}) \rangle = 3.73 \times 10^{-42}\ \mathrm{cm}^2, \tag{36}$$

for the neutral-current capture. The effective cross sections in Eq. (35) are valid for SN neutrinos without oscillations. When neutrino oscillations are taken into account, the oscillations of higher energy ν_x into ν_e result in an increased event rate since the expected ν_e energies in the absence of oscillations are just at or below the charged-current reaction threshold. This leads to an increase by a factor of 35 for the cross section $\langle \sigma(^{12}\mathrm{C}(\nu_e, e^-)^{12}\mathrm{N}) \rangle$ if we average it over a ν_e distribution with $T = 8$ MeV rather than 3.5 MeV. Similarly, the cross section $\langle \sigma(^{12}\mathrm{C}(\bar{\nu}_e, e^+)^{12}\mathrm{B}) \rangle$ is increased by a factor of 5.

In order to reduce the uncertainties of the unknown parameters appearing in the SN neutrino fluxes, including those in the luminosities L_α^0, temperatures T_α, and pinching parameters η_α, we define the ratio $R_1^{+(-)}$ as the event number of $\nu_e(\bar{\nu}_e)$ for the charged-current reaction detected after 1 s over that detected before 1 s,

$$R_1^{+(-)} = \frac{N^{CC}_{\nu_e(\bar{\nu}_e)}(1\ \mathrm{s} < t < 10\ \mathrm{s})}{N^{CC}_{\nu_e(\bar{\nu}_e)}(0 < t < 1\ \mathrm{s})}. \tag{37}$$

With Eqs. (1), (4), (14)–(17), (19)–(33), and (37), we can see that $R_1^{\pm}$ depends on the mixing angle θ_{13} and the luminosity decay time τ. From a detailed numerical calculation, we found that $R_1^{\pm}$ which changes with θ_{13} has also a significant dependence on τ. This can lead to large uncertainties in $R_1^{\pm}$ when τ varies in the range given in Eq. (2). Therefore, it will be difficult to identify the mass hierarchy and acquire information on θ_{13} from $R_1^{\pm}$ when τ has a significant uncertainty. However, if the value of $R_1^{\pm}$ is determined through SN neutrinos, we can obtain a rather tight relation between τ and θ_{13}. We demonstrate this relation in Fig. 6, for the neutrino-carbon reactions. In Fig. 6 we plot τ as a function of θ_{13} for a fixed value of R_1^+. We take $R_1^+ = 2.4$ and $L^0_{\nu_e}/L^0_{\nu_x} = 1$ as an example.[3] From this figure, we see that the value of τ lies in a small range, i.e., 2.68–3.00 when θ_{13} varies from 0 to 3° for the normal mass hierarchy. This is much smaller than the presently allowed range given in Eq. (2). It should be remarked that several authors [13,16,17] have typically used the best fit value, i.e., $\tau = 3$ s [22] in their study of SN neutrinos.

First consider the channel of the inverse beta decay in which only R_1^- is relevant. We plot R_1^- in Fig. 7 as a function of θ_{13} for the two mass hierarchies, and for

[3]We have checked that when $R_1^{\pm}$ and $L^0_{\nu_e}/L^0_{\nu_x}$ take other values, the qualitative results do not change.

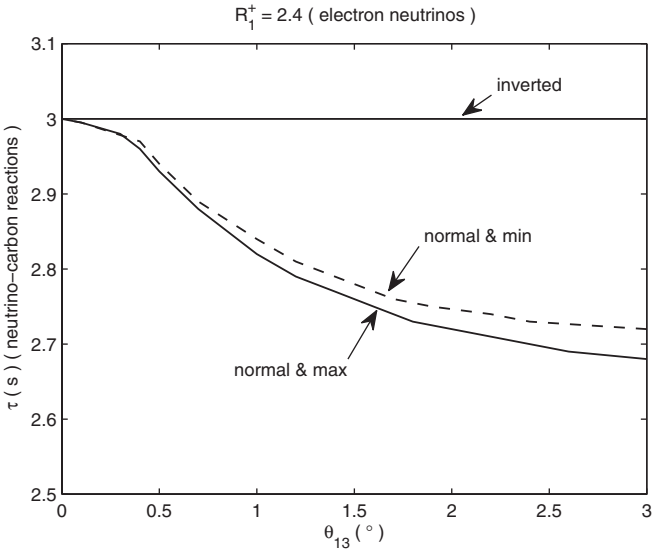

FIG. 6. The luminosity decay time τ as a function of the mixing angle θ_{13} in the channel of neutrino-carbon reactions at Daya Bay when $R_1^+ = 2.4$ and $L^0_{\nu_e}/L^0_{\nu_x} = 1$. The "max" ("min") corresponds to the maximum (minimum) values of T_α and η_α.

$L^0_{\nu_e}/L^0_{\nu_x}$, T_α, and η_α taking their allowed extreme values in the ranges given in Eqs. (3) and (5). For the normal mass hierarchy R_1^-, having the value of 2.4, is independent of θ_{13}. So it is impossible to obtain any information on θ_{13} for the normal mass hierarchy in the inverse beta decay process. For the inverted mass hierarchy, for a given value of

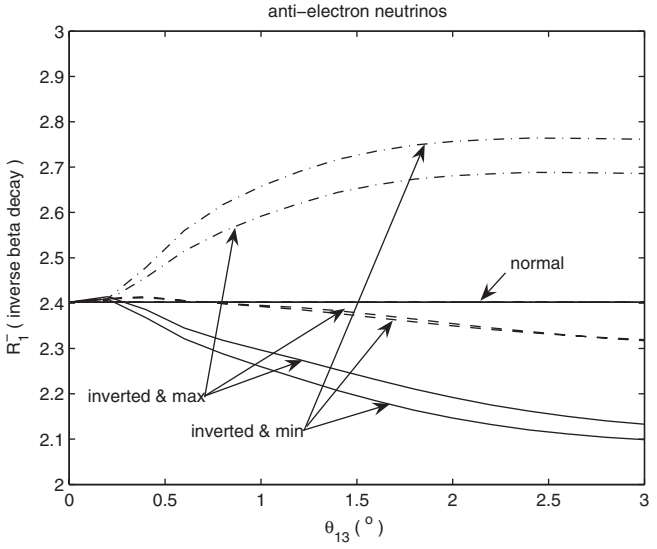

FIG. 7. The ratio R_1^- of the event number of $\bar{\nu}_e$ for the charged-current reaction detected after 1 s over that detected before 1 s, as a function of the mixing angle θ_{13} in the channel of inverse beta decay at Daya Bay. The solid curves correspond to $L^0_{\nu_e}/L^0_{\nu_x} = 1/2$, the dashed curves $L^0_{\nu_e}/L^0_{\nu_x} = 1$, and the dot-dashed curves $L^0_{\nu_e}/L^0_{\nu_x} = 2$. The "max" ("min") corresponds to the maximum (minimum) values of T_α and η_α.

$L_{\bar{\nu}_e}/L_{\bar{\nu}_x}$, R_1^- lies in a band bounded by the curves marked as "inverted & max" and "inverted & min," which are obtained by setting the values of both T_α and η_α at their upper and lower bounds, respectively. From this plot, it can be seen that if the value of R_1^- is away from 2.4, that is statically significant, the mass hierarchy must be inverted and a band of values of θ_{13} and $L_{\bar{\nu}_e}/L_{\bar{\nu}_x}$ can be determined. But it is difficult to determine θ_{13} from R_1^- alone. It is interesting to observe that, since the value of R_1^- falls, bound in the limited range of 2.1–2.8, it can serve as a test of the validity of the overall parametrization of the SN explosion mechanism.

For the neutrino-carbon reactions, both R_1^+ and R_1^- can be used to identify the mass hierarchy and obtain information on θ_{13}. In Fig. 8(a), we plot R_1^+ vs θ_{13} similar to Fig. 7. Here for the inverted mass hierarchy, R_1^+ has the constant value 2.4 independent of θ_{13}. If R_1^+ is larger than 2.4, the mass hierarchy must be normal. It can also be seen from Fig. 8(a) that R_1^+ depends on θ_{13} sensitively for the normal mass hierarchy and the uncertainties of R_1^+ due to L^0_α, T_α, and η_α are small. Therefore, in the case of normal mass hierarchy, we can restrict θ_{13} to a small range of values by measuring R_1^+. Similar plots are made for R_1^- in Fig. 8(b). Now for the normal mass hierarchy, R_1^- is independent of θ_{13}. For the inverted mass hierarchy R_1^- varies with θ_{13} and is smaller than 2.4. Hence we may also be able to identify the mass hierarchy by R_1^-. However, as shown in the plot, in the case of inverted mass hierarchy the large uncertainties of R_1^- due to L^0_α, T_α, and η_α make it difficult to constrain θ_{13} by R_1^-.

The Daya Bay experiment has the sensitivity limit of 0.01 for $\sin^2 2\theta_{13}$, i.e., 3° for θ_{13}. However, if a SN explosion takes place during the operation of the experiment, it is possible to reach a much smaller value of θ_{13} with the benefit of determining the mass hierarchy by measuring R_1^+ for the neutrino-carbon reactions.

Now let us consider the heavy water detector, for an example, used in the previous SNO experiment [19]. The detector mass was made of 1000 tons of heavy water located in the depth of $h = 6000$ mwe [4] [19,51]. We consider only the neutrino-deuterium reactions. The total number of deuterium is $N_T^{(d)} = 6.02 \times 10^{31}$. Scaling the experimentally measured energy values from the decay of the muon at rest to the energy scale of SN neutrinos, one can obtain the effective cross sections of neutrino-deuterium reactions as follows [50,52]:

$$\langle \sigma(d(\nu_e, e^-)pp) \rangle = (3.35 T_{\nu_e}^{2.31} - 3.70) \times 10^{-43}\ \text{cm}^2,$$
$$\langle \sigma(d(\bar{\nu}_e, e^+)nn) \rangle = (3.05 T_{\bar{\nu}_e}^{2.08} - 7.82) \times 10^{-43}\ \text{cm}^2, \quad (38)$$

for the charged-current capture, and

[4] mwe means meter-water-equivalent and 1 m of rock is about 2.7 m of water.

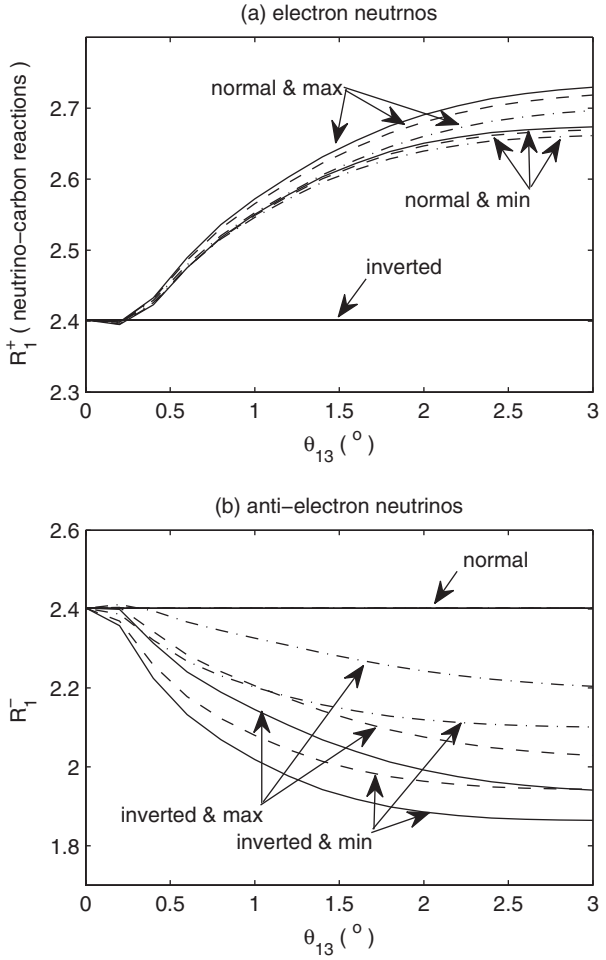

FIG. 8. (a) Similar to Fig. 7 but the electron neutrinos ν_e are observed in the channel of neutrino-carbon reactions at Daya Bay; (b) similar to Fig. 7 but the antielectron neutrinos $\bar{\nu}_e$ are observed in the channel of neutrino-carbon reactions at Daya Bay.

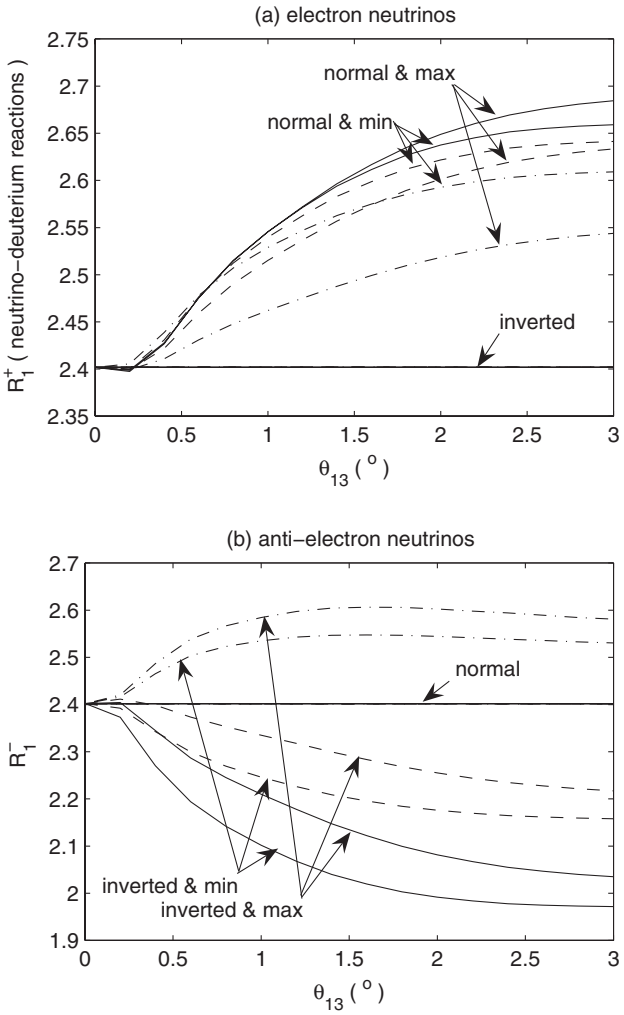

FIG. 9. (a) Similar to Fig. 7 but the electron neutrinos ν_e are observed in the channel of neutrino-deuterium reactions at SNO; (b) similar to Fig. 7 but the antielectron neutrinos $\bar{\nu}_e$ are observed in the channel of neutrino-deuterium reactions at SNO.

$$\langle\sigma(d(\nu_\alpha, \nu_\alpha)np)\rangle = (1.63T_{\nu_\alpha}^{2.26} - 2.78) \times 10^{-43}\ \text{cm}^2,$$
$$\langle\sigma(d(\bar{\nu}_\alpha, \bar{\nu}_\alpha)np)\rangle = (2.03T_{\bar{\nu}_\alpha}^{2.05} - 3.76) \times 10^{-43}\ \text{cm}^2, \quad (39)$$

for the neutral-current capture, where $\alpha = e, \mu, \tau$.

In Figs. 9(a) and 9(b) we plot R_1^+ and R_1^- of the neutrino-deuterium reactions in analogy with Figs. 8(a) and 8(b). Similar to the neutrino-carbon case given in Fig. 8(a), Fig. 9(a) for R_1^+ can be used to determine the neutrino mass hierarchy. But it is difficult to pin down the value of θ_{13}. Figure 9(b) for R_1^- is similar to Fig. 7 and the discussion can be applied to the present situation, with the allowed value of R_1^- between 1.9 to 2.6 in the case of inverted mass hierarchy.

In the above discussions, we have applied our method to three reactions: inverse beta decay, neutrino-carbon, and neutrino-deuterium. A summary is given in Table II. From this table, it can be seen that the mass hierarchy may be identified by measuring R_1^+ in the neutrino-carbon reactions and the neutrino-deuterium reactions, and by measuring R_1^- in the inverse beta decay, the neutrino-carbon reactions, and the neutrino-deuterium reactions. In addition, in the case of normal mass hierarchy, R_1^+ measured in the channel of neutrino-carbon reactions can provide the most accurate information about θ_{13}. Similarly, the present method can also be applied to other neutrino experiments, such as KamLAND [53], MiniBooNE [54], Borexino [55], and Double-Chooz [56] in the channel of neutrino-carbon reactions. In the future, if a SN explosion takes place within the cosmic distance considered here, it is possible to identify the mass hierarchy and reach a much smaller value of θ_{13} than current neutrino experiments through the measurement of R_1^+ in the channel of neutrino-carbon reactions.

TABLE II. Summary of measurement of the neutrino parameters by SN neutrinos in three reactions: the inverse beta decay, neutrino-carbon reactions, neutrino-deuterium reactions. "√" and "×" represent, respectively, the information can and cannot be obtained.

Reaction	Normal hierarchy ($\Delta m^2_{31} > 0$)	Inverted hierarchy ($\Delta m^2_{31} < 0$)	θ_{13} ($\leq 3°$)	Cosmic setting ($m_{\nu_\mu}, m_{\bar{\nu}_\mu}, m_{\nu_\tau}, m_{\bar{\nu}_\tau}$)	Figures
$\bar{\nu}_e + p$	×	√ ($R_1^- \neq 2.4$)	×	×	Figure 7
$\nu_\alpha + C$	√ ($R_1^+ > 2.4$)	×	√	√	Figures 8(a), 10(a), and 10(b)
$\bar{\nu}_\alpha + C$	×	√($R_1^- < 2.4$)	×	√	Figures 8(b), 10(a), and 10(b)
$\nu_\alpha + d$	√ ($R_1^+ > 2.4$)	×	×	√	Figures 9(a), 11(a), and 11(b)
$\bar{\nu}_\alpha + d$	×	√ ($R_1^- \neq 2.4$)	×	√	Figures 9(a), 11(a), and 11(b)

IV. CHECK NEUTRINO MASSES UNDER COSMIC SETTING

All of our understanding of neutrino properties has been derived in the terrestrial environment, with input from solar neutrinos, and our study of SN neutrinos has been made under the reasonable assumption that the terrestrial properties can be applied unaltered to the extreme conditions of the cosmos, such as those in the SN, e.g., high temperature, high density, etc. If an observation of SN neutrinos deviates from the prediction, it will be argued that our picture of SN requires modification. However, it would be prudent to check if some aspects of the properties of neutrinos may have been modified under the unusual cosmic conditions. In this section we propose a measurement, the observation of which can only be attributed to some change of the neutrino property, albeit a very specific one.

Since neutrinos, at least some of the species, have finite masses, their transmitting velocities are smaller than that of light. Then, neutrinos from a SN explosion, while traveling through a large distance to the Earth, can experience a delay in the arrival time, which depends on their energies and masses and may be observable [8,51,57].

Suppose a neutrino from a SN, of mass m (in eV) and energy E (in MeV), travels over a distance D (in 10 kpc) to the Earth; it will experience an energy-dependent time delay of Δt (in second) relative to a massless neutrino [8]:

$$\Delta t(\mathrm{s}) \backsimeq 0.5143\left(\frac{m\ (\mathrm{eV})}{E\ (\mathrm{MeV})}\right)^2 D(10\ \mathrm{kpc}), \tag{40}$$

where only the lowest-order term in the neutrino mass expansion has been kept. In Ref. [8], a method of measuring the neutrino mass is proposed, using the detection of the event number of the delayed SN neutrinos. In the papers, a simple model of the luminosities of SN neutrinos was assumed, in the absence of various effects considered in recent SN neutrino studies. The neutrino luminosities were assumed to have a common step-function cutoff at a fixed time. This form of luminosities was derived from the argument that the neutrino gravitational redshifts become severe enough only near the sharp cutoff time t_{BH}, where t_{BH} can be determined from the observed time profile of SN neutrinos. Therefore, the luminosities, which are constant before t_{BH} and vanishes abruptly afterward, take the form $L(t) = L^0_\alpha \theta(t_{BH} - t)$. In the present work, we take into account the full complexity of the neutrino flavor transformation due to the effects of the shock, MSW, collective, and the Earth matter. Also, we consider the time dependence of the SN neutrino luminosities given in Eq. (1) and the uncertainties in the SN neutrino flux parameters given in Eqs. (3) and (5). Since the time delay Δt depends on the neutrino mass m, we can express the event number of the delayed SN neutrinos as a function of m. Therefore, information about m can be obtained by detecting the event number of the delayed SN neutrinos.

From Ref. [58] there are the following neutrino mass bounds:[5]

$$m_{\bar{\nu}_e} < 2\ \mathrm{eV}, \qquad m_{\nu_\mu} < 0.19\ \mathrm{MeV}, \qquad m_{\nu_\tau} < 18.2\ \mathrm{MeV}. \tag{41}$$

For the SN electron antineutrino the averaged energy is $\langle E_{\bar{\nu}_e} \rangle \simeq 16$ MeV, which together with $D = 10$ kpc, gives $\Delta t_{\bar{\nu}_e} < 0.01$ s from Eq. (40). This time delay of the $\bar{\nu}_e$ is much smaller than the time scale of the SN explosion of about 10 s. And it is also too short to be observable. Similarly, for the electron neutrino $\langle E_{\nu_e} \rangle \simeq 11$ MeV, we find $\Delta t_{\nu_e} < 0.02$ s, which is again very short and much smaller than the time scale of SN explosion. Therefore, unless their effective mass is somehow significantly enhanced, ν_e and $\bar{\nu}_e$ can be considered as massless for the time delay observation. For the muon and tau neutrinos, according to the oscillation experiments their effective masses in the terrestrial setting will also be bound by 2 eV because of the much smaller values of Δm^2_{21} and Δm^2_{31},[6] their time delay will be very small too. In the following, we will tentatively ignore these terrestrial

[5]Note that these bounds are obtained from direct measurements of neutrino masses and they do not take into account neutrino oscillation experiments. The latter will relate neutrino effective masses of different flavors in a very tight range.

[6]The effective masses of the flavor neutrinos, m_α, $\alpha = e$, μ, and τ, to those of the regular neutrino masses, m_j, $j = 1$, 2, and 3, by

$$m_\alpha = \sum_{j=1,2,3} |U_{\alpha j}|^2 m_j,$$

where $U_{\alpha j}$ is the neutrino mixing matrix.

bounds to form the basis of our proposal for a test of neutrino properties under the cosmic setting of extreme conditions.

After the SN explosion the emission of different flavors of neutrinos lasts for a period of about 10 s. The arrival to the Earth of those flavors of neutrinos and antineutrinos whose effective masses are not affected will last about the same period of time. For other flavors which are affected there may be a delay in the arrival time, depending on the values of their effective masses. We look for measurements which are sensitive to both charge and neutral-current events, such as the detector types of the Daya Bay [9], LVD [59], and SNO [60] experiments, which involve the neutrino-carbon and neutrino-deuterium reactions. The experimental information that these detectors can potentially provide include the event numbers of the electron antineutrino from charged-current reactions and the total event number of all the three flavors of neutrinos from the neutral-current reactions. We shall assume that the electron neutrino mass is not affected so as to avoid any possibility of influencing the existing result of nucleosynthesis. But the effective masses of the muon and tau neutrinos might be affected. Then, there might be a time delay Δt_x between the charged-current events and some of the neutral-current events if the muon and tau flavors of SN neutrinos appear to have sufficiently sizable effective masses. Denoting the effective mass of ν_x (ν_μ, $\bar{\nu}_\mu$, ν_τ, or $\bar{\nu}_\tau$) by m_{ν_x}, we have

$$\Delta t_x = \langle t\rangle_{NC} - \langle t\rangle_{CC} \backsimeq 0.5143\left(\frac{m_x}{E}\right)^2 D, \qquad (42)$$

where we have dropped the units for Δt_x, m_x, E, and D as indicated in Eq. (40). $\langle t\rangle_{NC}$ is the average time of SN neutrinos of the neutral-current reactions to arrive at the detector and $\langle t\rangle_{CC}$ that of the charged-current reactions. A nonvanishing Δt_x signalizes a significantly larger effective mass for the muon or tau neutrino, independent of parameters of the SN and neutrinos.

To gain a sense of how Δt_x may look and how sensitive it is to the effective mass of the muon and tau neutrinos, we have to do some model calculation for quantities which can be measured in a SN neutrino experiment. We found that such a quantity is available as described below. We use the charged-current events which are from the electron antineutrino to monitor the events that are not delayed, and the neutral-current events which involve all flavors to measure the possible time delay. We divide the total neutral-current events into two groups: $N_{\rm total}^{NC(r)}$ and $N_{\rm total}^{NC(0)}$, where $N_{\rm total}^{NC(r)}$ is the total neutral-current events accompanying the charged-current events and are therefore not delayed, and $N_{\rm total}^{NC(0)}$ are all the total neutral-current events including both delayed and not delayed. We define the event number of the delayed ν_x plus $\bar{\nu}_x$ from the neutral-current events as

$$N^{NC}(\text{delay}) = N_{\rm total}^{NC(0)} - N_{\rm total}^{NC(r)}.$$

The quantity to be measured is the new ratio,

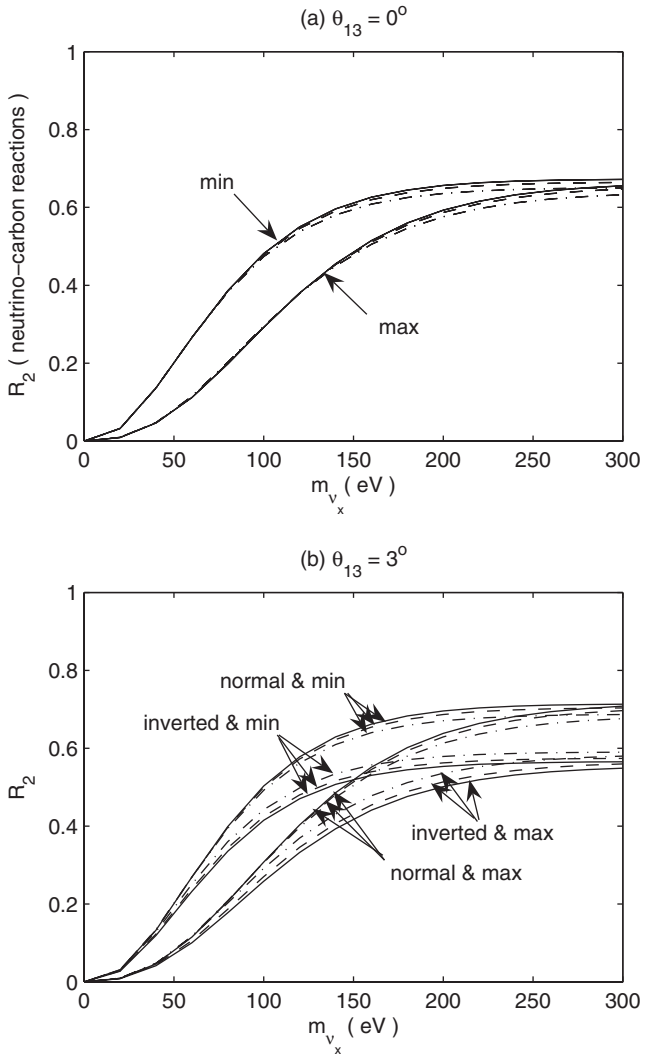

FIG. 10. For the neutral-current reactions R_2 in the channel of neutrino-carbon reactions at Daya Bay, the ratio of the event number of delayed neutrinos over the total event number, as a function of m_{ν_x} at two values of θ_{13}, each has the two mass hierarchies with $L^0_{\nu_e}/L^0_{\nu_x}$, T_α, and η_α taking their limiting values. The solid curves correspond to $L^0_{\nu_e}/L^0_{\nu_x} = 1/2$, the dashed curves $L^0_{\nu_e}/L^0_{\nu_x} = 1$, and the dot-dashed curves $L^0_{\nu_e}/L^0_{\nu_x} = 2$. The "max" ("min") corresponds to the maximum (minimum) values of T_α and η_α. Figure (a) shows that R_2 is nearly independent of $L^0_{\nu_e}/L^0_{\nu_x}$ and the mass hierarchy.

$$R_2 = \frac{N^{NC}(\text{delay})}{N_{\rm total}^{NC(0)}} = \frac{N_{\rm total}^{NC(0)} - N_{\rm total}^{NC(r)}}{N_{\rm total}^{NC(0)}}. \qquad (43)$$

This ratio is very insensitive to the values of Δm^2_{21} and Δm^2_{31}.[7] It should also be remarked that because of the ratio, the effect of the various uncertainties involved, such as the

[7]Our numerical simulation shows that R_2 is insensitive to variations of Δm^2_{21} and Δm^2_{31} in a range of 10 and 8 orders of magnitude, respectively.

neutrino and SN parameters, will be reduced in R_2. Using the charged-current events to monitor the undelayed neutral-current events will bypass the question of the uncertainty in the total emission time of SN neutrinos.

Since we cannot tag the flavor of neutral-current events the information on the masses of the muon and tau neutrinos are correlated. For the purpose of illustration we assume ν_μ and ν_τ to have the same effective mass. We keep all other features of neutrinos and the SN unchanged. For the neutrino-carbon reactions at Daya Bay, we plot in Fig. 10 two sets of curves which describe R_2 as a function of m_{ν_x}, each for a fixed value of θ_{13}. In Fig. 10(a) for $\theta_{13} = 0$, it can be seen that the curves are insensitive to $L^0_{\nu_e}/L^0_{\nu_x}$ and the mass hierarchy. For $m_{\nu_x} < 200$ eV, R_2 is sensitive to m_{ν_x}. A measurement of R_2 can restrict m_x in a distinctive range of values determined by the uncertainties in the SN neutrino temperature and chemical potential. In Fig. 10(b) for $\theta_{13} = 3°$, R_2 is again shown to be sensitive to m_x for $m_{\nu_x} < 200$ eV. The two mass hierarchies overlap for small m_x but fall into well-separated regions for $m_x > 200$ eV.

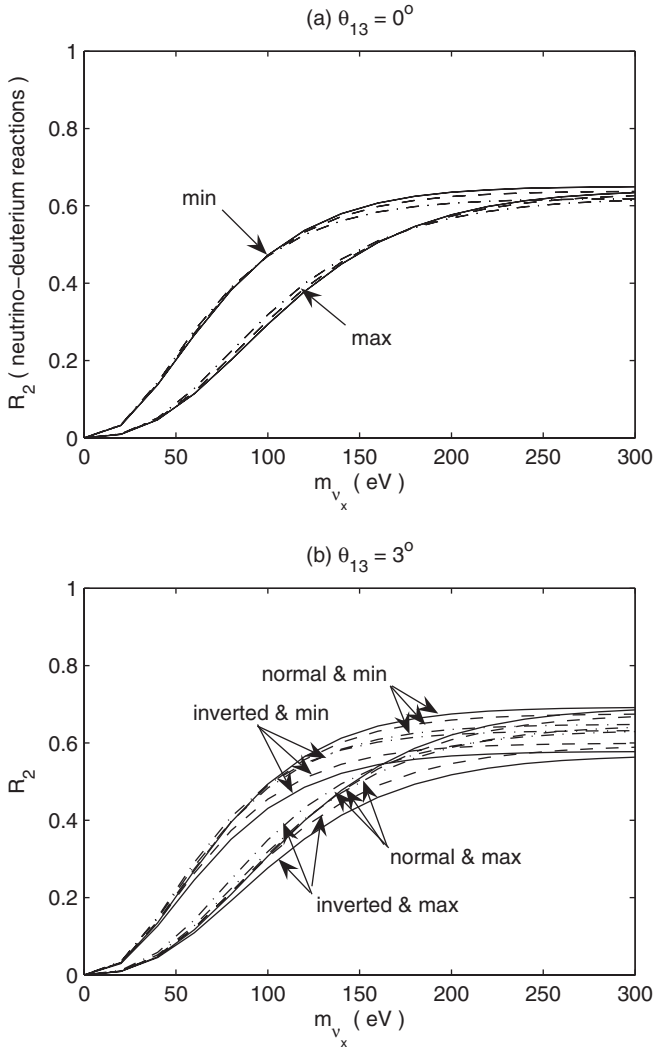

FIG. 11. Similar to Fig. 10 but in the channel of neutrino-deuterium reactions at SNO.

In Figs. 11 we plot R_2 for the neutrino-deuterium reactions in analogy to Figs. 11 of the neutrino-carbon reactions. Figure 11(a) is very similar to Fig. 10(a). Figure 11(b) is also similar to Fig. 10(b) for m_{ν_x} smaller than 150 eV, but there are some differences at larger m_x. In this latter case, unlike Fig. 10(b), Fig. 11(b) shows that the two mass hierarchies can no longer be separated even for m_{ν_x} greater than 200 eV.

The method can also be applied to KamLAND, MiniBooNE, Borexino, and Double-Chooz in the channel of neutrino-carbon reactions, and the results are similar to those given for the Daya Bay experiment.

V. DISCUSSION AND SUMMARY

In this paper, we considered the SN shock effects, the MSW effects, the collective effects, and the Earth matter effects in the detection of type II SN neutrinos. Also, we considered the uncertainties in the neutrino luminosities L^0_α, their temperatures T_α, and their pinching parameters η_α in the calculation of different flavors of SN neutrinos. We found that quantities suitably defined in terms of event numbers of different flavors of SN neutrinos are sensitive to the neutrino mass hierarchy, the mixing angle θ_{13}, and neutrino masses. Therefore, it is possible to identify the mass hierarchy, acquire information about θ_{13}, and look into certain neutrino mass patterns of SN neutrinos.

First, we defined the ratio $R_1^{+(-)}$ as the event number of $\nu_e(\bar{\nu}_e)$ for the charged-current reaction detected after 1 s over that detected in the first 1 s, and discussed the dependence of $R_1^{+(-)}$ on θ_{13} for different mass hierarchies. With this, we may identify the mass hierarchy and obtain information about θ_{13}. This method can be applied to several detector types relying on specific physical processes, including the inverse beta decay (Fig. 7), neutrino-carbon reactions [Figs. 8(a) and 8(b)], and neutrino-deuterium reactions [Figs. 9(a) and 9(b)]. From our numerical calculations, the mass hierarchy may be identified by measuring R_1^+ in the neutrino-carbon reactions and the neutrino-deuterium reactions, R_1^- in the inverse beta decay, the neutrino-carbon reaction, and the neutrino-deuterium reactions. In addition, in the case of normal mass hierarchy, R_1^+ measured in the neutrino-carbon reactions provides the most restrictive information about θ_{13}. Therefore, we can both identify the mass hierarchy and measure θ_{13} from R_1^+ in the channel of neutrino-carbon reactions at several experiments such as Daya Bay, KamLAND, MiniBooNE, Borexino, and Double-Chooz.

Second, we defined another ratio, R_2, for the neutral-current reactions, as the event number of the delayed neutrinos over the total event number, with the charge current events as a monitor of undelayed events. The significance of R_2 is that it offers a possibility to detect a

possible difference between the electron neutrino and its other flavor counterparts, in particular, any significant difference in their effective masses under the cosmic setting of extreme conditions. With the plot of R_2 vs m_{ν_x}, we can study m_{ν_x} vs m_{ν_e}. This method is applied to both neutrino-carbon and neutrino-deuterium reactions and the result is given, respectively, in Figs. 10 and 11. What we have presented for R_2 is a case study with rather restricted input. In case there is an indication of nonvanishing R_2 a detailed refined calculation should be made.

In conclusion, if a SN explosion takes place within the cosmic distance considered here, it is possible to identify the mass hierarchy and obtain information on θ_{13}. With suitable setup of the detector, a study of some unusual properties of neutrinos under the cosmic setting is possible. A summary of the detector types and their capabilities in association with the studies presented in this article is given in Table II.

ACKNOWLEDGMENTS

We would like to thank F.-G. Cao and C.-G. Yang for helpful discussions. This work was supported in part by National Natural Science Foundation of China (Project Nos. 10535050, 10675022, 10975018, and 10890092) and the Special Grants from Beijing Normal University.

[1] K. Kotake, K. Sato, and K. Takahashi, Rep. Prog. Phys. **69**, 971 (2006).
[2] K. Hirata *et al.*, Phys. Rev. Lett. **58**, 1490 (1987); R. M. Bionta *et al.*, Phys. Rev. Lett. **58**, 1494 (1987); V. Trimble, Rev. Mod. Phys. **60**, 859 (1988); W. D. Arnett, J. N. Bahcall, R. P. Kirshner, and S. E. Woosley, Annu. Rev. Astron. Astrophys. **27**, 629 (1989); W. Hillebrandt and P. Höflich, Rep. Prog. Phys. **52**, 1421 (1989); D. N. Schramm, Phys. Rep. **189**, 89 (1990); M. Koshiba, Phys. Rep. **220**, 229 (1992); R. McCray, Annu. Rev. Astron. Astrophys. **31**, 175 (1993).
[3] A. Dighe, J. Phys. Conf. Ser. **136**, 022041 (2008); AIP Conf. Proc. **981**, 75 (2008).
[4] X.-H. Guo, M.-Y. Huang, and B.-L. Young, Chin. Phys. C **34**, 257 (2010).
[5] G. G. Raffelt, *Stars as Laboratories for Fundamental Physics* (University of Chicago, Chicago, 1996).
[6] B. Dasgupta, A. Dighe, and A. Mirizzi, Phys. Rev. Lett. **101**, 171801 (2008).
[7] S. Skadhauge and R. Z. Funchal, J. Cosmol. Astropart. Phys. 04 (2007) 014.
[8] J. F. Beacom, R. N. Boyd, and A. Mezzacappa, Phys. Rev. Lett. **85**, 3568 (2000); Phys. Rev. D **63**, 073011 (2001).
[9] X.-H. Guo *et al.* (Daya Bay Collaboration), arXiv:hep-ex/0701029.
[10] P. Antonioli *et al.*, New J. Phys. **6**, 114 (2004).
[11] X.-H. Guo, M.-Y. Huang, and B.-L. Young, Phys. Rev. D **79**, 113007 (2009).
[12] B. Dasgupta and A. Dighe, Phys. Rev. D **77**, 113002 (2008); S. Chakraborty, S. Choubey, B. Dasgupta, and K. Kar, J. Cosmol. Astropart. Phys. 09 (2008) 013.
[13] J. P. Kneller, G. C. McLaughlin, and J. Brockman, Phys. Rev. D **77**, 045023 (2008).
[14] H.-Y. Duan, G. M. Fuller, and J. Carlson, Comp. Sci. Disc. **1**, 015007 (2008).
[15] J. R. Wilson, *Numerical Astrophysics*, edited by J. M. Centrella, J. M. LeBlanc, and R. L. Bowers (Jones and Bartlett, Boston, 1985), p. 422–434; J. R. Wilson, R. W. Mayle, S. E. Woosely, and A. T. Weaver, Ann. N.Y. Acad. Sci. **470**, 267 (1986).
[16] R. C. Schirato and G. M. Fuller, arXiv:astro-ph/0205390.
[17] G. L. Fogli, E. Lisi, A. Mirizzi, and D. Montanino, Phys. Rev. D **68**, 033005 (2003).
[18] M. T. Keil, G. G. Raffelt, and H.-T. Janka, Astrophys. J. **590**, 971 (2003); G. G. Raffelt, M. T. Keil, R. Buras, H.-T. Janka, and M. Rampp, arXiv:astro-ph/0303226.
[19] J. Boger *et al.*, Nucl. Instrum. Methods Phys. Res., Sect. A **449**, 172 (2000).
[20] C. Giunti and C. W. Kim, *Fundamentals of Neutrino Physics and Astrophysics* (Oxford, New York, 2007); S. L. Shapiro and S. A. Teukolsky, *Black Holes, White Dwarfs, and Neutron Stars* (Wiley, New York, 1983); R. N. Mohapatra and P. B. Pal, *Massive Neutrino in Physics and Astrophysics* (World Scientific, Singapore, 2004), 3d ed..
[21] D. N. Spergel, T. Piran, A. Loeb, J. Goodman, and J. N. Bahcall, Science **237**, 1471 (1987).
[22] T. J. Loredo and D. Q. Lamb, Ann. N.Y. Acad. Sci. **571**, 601 (1989); Phys. Rev. D **65**, 063002 (2002).
[23] Y. Totsuka, Rep. Prog. Phys. **55**, 377 (1992).
[24] J. R. Wilson and R. W. Mayle, Phys. Rep. **163**, 63 (1988); **227**, 97 (1993).
[25] T. Totani, K. Sato, H. E. Dalhed, and J. R. Wilson, Astrophys. J. **496**, 216 (1998).
[26] H.-T. Janka and W. Hillebrandt, Astron. Astrophys. **224**, 49 (1989); Astron. Astrophys. Suppl. Ser. **78**, 375 (1989); H.-T. Janka, Astron. Astrophys. **244**, 378 (1991).
[27] G. L. Fogli, E. Lisi, A. Mirizzi, and D. Montanino, J. Cosmol. Astropart. Phys. 04 (2005) 002; 06 (2006) 012.
[28] C. Lunardini and A. Y. Smirnov, J. Cosmol. Astropart. Phys. 06 (2003) 009.
[29] K. Takahashi, K. Stao, H. E. Dalhed, and J. R. Wilson, Astropart. Phys. **20**, 189 (2003); R. Tomàs, M. Kachelrieβ, G. G. Raffelt, A. Dighe, H.-T. Janka, and L. Scheck, J. Cosmol. Astropart. Phys. 09 (2004) 015.
[30] L. Wolfenstein, Phys. Rev. D **17**, 2369 (1978); **20**, 2634 (1979); S. P. Mikheyev and A. Y. Smirnov, Yad. Fiz. **42**, 1441 (1985) [Sov. J. Nucl. Phys. **42**, 913 (1985)]; Nuovo Cimento Soc. Ital. Fis. C **9**, 17 (1986); Zh. Eksp. Teor. Fiz. **91**, 7 (1986) [Sov. Phys. JETP **64**, 4 (1986)]; Usp. Fiz.

Nauk **153**, 3 (1987) [Sov. Phys. Usp. **30**, 759 (1987)]; Prog. Part. Nucl. Phys.**23**, 41 (1989).
[31] T. K. Kuo and J. Pantaleone, Rev. Mod. Phys. **61**, 937 (1989); Phys. Rev. D **39**, 1930 (1989).
[32] A. Yu. Smirnov, Phys. Scr. **T121**, 57 (2005); arXiv:hep-ph/0702061.
[33] H.-Y. Duan and J. P. Kneller, J. Phys. G **36**, 113201 (2009).
[34] H.-Y. Duan, G. M. Fuller, and Y.-Z. Qian, Phys. Rev. D **74**, 123004 (2006); **76**, 085013 (2007); H.-Y. Duan, G. M. Fuller, J. Carlson, and Y.-Z. Qian, Phys. Rev. D **75**, 125005 (2007); Phys. Rev. Lett. **99**, 241802 (2007).
[35] H.-Y. Duan, G. M. Fuller, and Y.-Z. Qian, J. Phys. G **36**, 105003 (2009).
[36] H.-Y. Duan, G. M. Fuller, and Y.-Z. Qian, arXiv:1001.2799.
[37] S. Hannestad, G. G. Raffelt, G. Sigl, and Y. Y. Y. Wong, Phys. Rev. D **74**, 105010 (2006); **76**, 029901 (2007).
[38] G. G. Raffelt and A. Y. Smirnov, Phys. Rev. D **76**, 081301 (R) (2007); **76**, 125008 (2007).
[39] G. L. Fogli, E. Lisi, A. Mirizzi, and D. Montanino, J. Cosmol. Astropart. Phys. 12 (2007) 010; G. L. Fogli, E. Lisi, A. Mirizzi, and I. Tamborra, J. Cosmol. Astropart. Phys. 04 (2009) 030; 10 (2009) 002.
[40] A. S. Dighe and A. Y. Smirnov, Phys. Rev. D **62**, 033007 (2000).
[41] X.-H. Guo and B.-L. Young, Phys. Rev. D **73**, 093003 (2006).
[42] A. N. Ioannisian and A. Yu. Smirnov, Phys. Rev. Lett. **93**, 241801 (2004); A. N. Ioannisian, N. A. Kazarian, A. Yu. Smirnov, and D. Wyler, Phys. Rev. D **71**, 033006 (2005).
[43] C. Lunardini and A. Yu. Smirnov, Nucl. Phys. **B616**, 307 (2001); Phys. Rev. D **63**, 073009 (2001); E. K. Akhmedov, C. Lunardini, and A. Yu. Smirnov, Nucl. Phys. **B643**, 339 (2002).
[44] H. A. Bethe, Rev. Mod. Phys. **62**, 801 (1990); G. E. Brown, H. A. Bethe, and G. Baym, Nucl. Phys. **A375**, 481 (1982).
[45] L. D. Landau and E. M. Lifshitz, *Quantum Mechanics: Non-relativistic Theory* (Pergamon, New York, 1977); C. Zener, Proc. R. Soc. A **137**, 696 (1932).
[46] M. C. Gonzalez-Garcia and M. Maltoni, Phys. Rep. **460**, 1 (2008); T. Schwetz, M. Tortola, and J. W. F. Valle, New J. Phys. **10**, 113011 (2008).
[47] H Duan, G. M. Fuller, and J Carlson, Simulating Nonlinear Neutrino Flavor Evolution, http://iopscience.iop.org/1749-4699/1/1/015007/media.
[48] A. M. Dziewonski and D. L. Anderson, Phys. Earth Planet. Inter. **25**, 297 (1981); F. D. Stacey, *Physics of the Earth* (Wiley, New York, 1977), 2nd ed..
[49] L. Cadonati, F. P. Calaprice, and M. C. Chen, Astropart. Phys. **16**, 361 (2002).
[50] A. Burrows, S. Reddy, and T. A. Thompson, Nucl. Phys. **A777**, 356 (2006).
[51] J. F. Beacom and P. Vogel, Phys. Rev. D **58**, 093012 (1998); J. F. Beacom and L. E. Strigari, Phys. Rev. C **73**, 035807 (2006).
[52] N. Tatara, Y. Kohyama, and K. Kubodera, Phys. Rev. C **42**, 1694 (1990); S. Ying, W. C. Haxton, and E. M. Henley, Phys. Rev. D **40**, 3211 (1989); Phys. Rev. C **45**, 1982 (1992).
[53] J. Busenitz *et al.* (KamLAND Collaboration), Proposal for US Participation in KamLAND, 1999; J. Busenitz, Int. J. Mod. Phys. A **16**, 742 (2001); K. Eguchi *et al.*, Phys. Rev. Lett. **90**, 021802 (2003); T. Araki *et al.*, Nature (London) **436**, 499 (2005).
[54] S. J. Brice, Nucl. Instrum. Methods Phys. Res., Sect. A **562**, 97 (2006); A. A. Aguilar-Arevalo *et al.*, Phys. Rev. Lett. **98**, 231801 (2007).
[55] G. Alimonti *et al.*, Astropart. Phys. **16**, 205 (2002); M. Balata *et al.*, Eur. Phys. J. C **47**, 21 (2006).
[56] F. Ardellier *et al.*, arXiv:hep-ex/0606025; M. Apollonio *et al.*, Eur. Phys. J. C **27**, 331 (2003).
[57] J. F. Beacom and P. Vogel, Phys. Rev. D **58**, 053010 (1998); H. Yüksel, S. Ando, and J. F. Beacom, Phys. Rev. C **74**, 015803 (2006).
[58] C. Amsler *et al.* (Particle Data Group), Phys. Lett. B **667**, 1 (2008).
[59] N. Y. Agafonova *et al.*, Astropart. Phys. **27**, 254 (2007).
[60] Q. R. Ahmad *et al.*, Phys. Rev. Lett. **89**, 011301 (2002); S. N. Ahmed *et al.*, Phys. Rev. Lett. **92**, 181301 (2004); B. Aharmim *et al.*, Phys. Rev. C **75**, 045502 (2007).